Phys. Status Solidi B **247**, Nos. 11–12, 2935–2940 (2010) / **DOI** 10.1002/pssb.201000347

physica status solidi b
www.pss-b.com
basic solid state physics

Hyperfine interaction in graphene: The relevance for spintronics

Balázs Dóra[*,1] **and Ferenc Simon**[2]

[1] Department of Physics, Budapest University of Technology and Economics, 1521 Budapest, Hungary
[2] Fakultät für Physik, Universität Wien, Strudlhofgasse 4, 1090 Wien, Austria

Received 20 May 2010, revised 21 July 2010, accepted 27 July 2010
Published online 20 September 2010

Keywords graphene, nuclear magnetic resonance, Knight shift

[*] Corresponding author: e-mail dora@kapica.phy.bme.hu, Phone: +36-1-463-3827, Fax: +36-1+463-4180

We study the nuclear magnetic resonance (NMR) properties of graphene. The interaction between nuclear spins and the orbital motion of Dirac electrons is strongly modified by the linear electronic dispersion with respect to its canonical form. The NMR shift and spin-lattice relaxation time are calculated as function of temperature, chemical potential, and magnetic field for clean and impure graphene, and three distinct regimes are identified: Fermi-, Dirac-gas, and extreme quantum limit (EQL) behaviors. A critical spectrometer assessment shows that NMR is within reach for fully ^{13}C enriched graphene of reasonable size.

1 Introduction Nuclear magnetic resonance (NMR) is a powerful analytical tool [1, 2] and an architecture for quantum information processing [3, 4] at the same time. Both of these applications are possible due to the relatively weak interaction of the nucleus with its environment. When employed as an analytical tool, this weak interaction is sufficient to probe the electronic state of its vicinity, which yields information about the local electron bonds or about the correlated behavior of electrons as *e.g.*, in superconductors [5]. NMR quantum computing exploits that the nuclei are well isolated from the environment thus there is a longer time window for the manipulation and detection of the nuclear quantum state.

For both kinds of applications, the important NMR measurables are the shift of the NMR resonance with respect to a standard, and the decay of the longitudinal magnetization to its equilibrium value, the spin-lattice relaxation time, T_1. These have been extensively studied in solid state systems both theoretically and experimentally [1, 6]. However, the body of NMR experiments and theory were focused on the behavior of three-dimensional systems which stemmed from the unavailability of stable, inherently two-dimensional materials, and from the relatively weak sensitivity of NMR spectroscopy.

The isolation of graphene, a single sheet of carbon atoms in a hexagonal lattice [7], enables studies of an exactly two-dimensional system. Its quasiparticles follow a linear band dispersion, causing the electrons to behave as massless Dirac fermions, which gives rise to unique transport and magnetic properties [8]. An important property of graphene is that its Fermi energy, E_F and the corresponding density of states (DOS) on the Fermi surface can be altered by a bias or by chemical doping which greatly affects its properties.

The NMR measurables are most affected by the surrounding electrons through the the electron-nuclear hyperfine interaction (HFI). The standard, text-book form of the HFI of nuclei and conduction electrons leads to the Hamiltonian [6]:

$$H_{\mathrm{HFI}} = \frac{\mu_0}{4\pi} g\hbar\gamma_{\mathrm{n}} \boldsymbol{I}\left[\mu_{\mathrm{B}}^{*}\frac{\boldsymbol{r}\times\boldsymbol{p}}{\hbar r^3} + \mu_{\mathrm{B}}\left(\frac{\boldsymbol{S}r^2 - 3r(\boldsymbol{S}r)}{r^5} - \frac{8\pi}{3}\boldsymbol{S}\delta(\boldsymbol{r})\right)\right]. \quad (1)$$

Here, the first term is due to the electron orbital magnetism, the second is due to the electron spin-dipole interaction, and the third is the so-called Fermi-contact interaction. μ_0 is the permeability of free space, γ_{n} the nuclear gyromagnetic ratio, $\boldsymbol{I}$ the nuclear spin, $g \approx 2$ the g-factor of the electrons. $\boldsymbol{S}$, $\boldsymbol{p}$, and $\boldsymbol{r}$ are the electron spin, momentum, and vector operators. μ_{B} is the Bohr magneton and $\mu_{\mathrm{B}}^{*} = m/m^{*}\mu_{\mathrm{B}}$ is the effective orbital Bohr magneton [9], where m^{*} is the effective band mass and m is the mass of a free electron.

We derive the hyperfine Hamiltonian for graphene, paying special attention to the orbital and spin contributions. Based on this, we calculate the Kinght shift and the spin-lattice relaxation time. We also discuss the feasibility of bulk NMR spectroscopy on graphene.

2 Electron–nucleus interaction The interaction between the nuclear spins and conduction electrons is most readily formulated following Abragam [6] by treating the nucleus as a magnetic dipole with $\boldsymbol{m} = \hbar\gamma_n \boldsymbol{I}$, and investigating its effect on the conduction electrons by introducing the kinetic momentum as $\boldsymbol{p} \to \boldsymbol{p} + e\boldsymbol{A}$ and through the Zeeman term. The vector potential created by the nuclear dipole is

$$\boldsymbol{A}(\boldsymbol{r}) = \frac{\mu_0}{4\pi}\frac{\boldsymbol{m}\times\boldsymbol{r}}{r^3}, \tag{2}$$

This gives rise to an interaction between the nuclear spin and the orbital motion and spin of the conduction electrons. The Hamiltonian accounting for the low-energy excitations of graphene around the K point is the two-dimensional Dirac equation, given by [8]

$$H = v_F\left(\sigma_x p_x + \sigma_y p_y\right), \tag{3}$$

where $v_F = 10^6$ m/s is the Fermi velocity of graphene, and the pseudospin variables (Pauli matrices, σ) spring from the two-sublattice structure of the honeycomb lattice (Fig. 1). Its eigenenergy is $E_\alpha(\boldsymbol{k}) = \alpha\hbar v_F|k|$, where $\alpha = \pm$ corresponds to the conduction and valence band (upper and lower Dirac cone). The corresponding eigenfunction is

$$\phi_{\alpha k}(\boldsymbol{r}) = \frac{1}{\sqrt{2NA_c}}\exp(i\boldsymbol{k}\boldsymbol{r})\begin{bmatrix}\alpha\\ \exp(i\varphi_k)\end{bmatrix}, \tag{4}$$

φ_k is the angle of $\boldsymbol{k}$ with the k_x axis, $A_c = 3\sqrt{3}a^2/2 \approx 5.24\times10^{-20}\,\mathrm{m}^2$ is the area of the unit cell, $a = 1.42$ Å is the C–C bond length, N is the number of unit cells. Since only the x and y components of the momentum appear here, it suffices to determine the corresponding components of the vector potential: $A_x = -\frac{\mu_0}{4\pi}m_z y/r^3$ and $A_y = \frac{\mu_0}{4\pi}m_z x/r^3$. Substituting this into the Dirac Hamiltonian, Eq. (3), we get for the effective Hamiltonian describing the electron–nucleus interactions as

$$H_{\mathrm{HFI,graphene}} = \frac{\mu_0}{4\pi}\hbar\gamma_n I_z\left(\frac{\boldsymbol{r}\times\boldsymbol{j}}{r^3}\right)_z + \frac{\mu_0}{4\pi}g\mu_B\hbar\gamma_n\boldsymbol{I}\left(\frac{\boldsymbol{S}r^2-3\boldsymbol{r}(\boldsymbol{S}\boldsymbol{r})}{r^5}-\frac{8\pi}{3}\boldsymbol{S}\delta(\boldsymbol{r})\right), \tag{5}$$

where $\boldsymbol{j} = ev_F\boldsymbol{\sigma}$ is the electric current operator in graphene. Here, $\boldsymbol{\sigma}$ is a vector of the Pauli matrices. The first term describes the interaction of the nucleus with the orbital motion of the Dirac electrons [10], and since the motion of the electrons is restricted in the $x-y$ plane, the orbital magnetization, $\boldsymbol{r}\times\boldsymbol{j}$ is perpendicular to it, thus interacts only with I_z. The spin-dipole and Fermi contact terms are unchanged.

The orbital term in Eq. (5) differs significantly from the usual form, Eq. (1). First, the numerical prefactors are different and second, the operator form of the interaction is different: the orbital magnetization ($\boldsymbol{r}\times\boldsymbol{j}$) replaces the angular momentum operator ($\boldsymbol{r}\times\boldsymbol{p}$). The peculiar form of the current operator for Dirac electrons $\boldsymbol{j}\sim\sigma$ is responsible for the jittery motion of the center of mass coordinate known as Zitterbewegung [11], and this also determines the orbital part of the interaction. Eq. (1) can be deduced formally from Eq. (5) by using $\boldsymbol{j} = e\boldsymbol{p}/m^*$ for a normal metal.

A unique property of the orbital magnetic moment of graphene is, that it remains invariant in an applied magnetic or gauge field. In a normal metal, the angular momentum operator and the corresponding orbital magnetic moment are gauge dependent through the introduction of a vector potential, $\boldsymbol{p} \to \boldsymbol{p} + e\boldsymbol{A}(\boldsymbol{r})$. As a result, the usual angular momentum operator contains a term proportional to the applied magnetic field, yielding additional contributions to the nuclear spin relaxation [12]. In graphene, however, this term is not present and the form of $\boldsymbol{j}$ is insensitive to the vector potential. We mention that the proper orbital angular momentum of Dirac particles is still $\boldsymbol{r}\times\boldsymbol{p}$ in the sense that it is responsible for rotations in the $x-y$ plane, which differs from the orbital magnetization.

The linearity of the Dirac equation in momentum also implies that there are no higher order terms in the vector potential [*e.g.*, $\boldsymbol{A}(\boldsymbol{r})^2$, which naturally occurs for the quadratic dispersion], and therefore an effective interaction between nuclear spins mediated by conduction electrons does not exist.

The second quantized form of the orbital part of the interaction is obtained using the eigenfunctions of the Dirac equation, Eq. (4). Its matrix elements are given by

$$\int \mathrm{d}\boldsymbol{r}\phi^*_{\alpha'k'}(\boldsymbol{r})\left(\frac{x\sigma_y - y\sigma_x}{r^3}\right)\phi_{\alpha k}(\boldsymbol{r}) = \int\frac{\mathrm{d}x\mathrm{d}y}{2NA_c}\frac{\exp(i(\boldsymbol{k}-\boldsymbol{k}')\boldsymbol{r})}{r^3} \times\left[-\alpha'\exp(i\varphi_k)(y+ix)+\alpha\exp(-i\varphi_{k'})(ix-y)\right]. \tag{6}$$

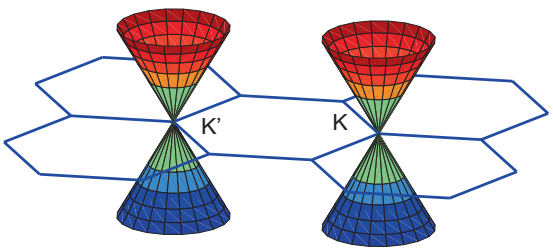

Figure 1 (online color at: www.pss-b.com) The two non-equivalent Dirac cones are shown on the honeycomb lattice. The non-equidistant equienergy levels denote the Landau level structure in perpendicular magnetic field.

Thus, we are left with integrals of the type

$$\mathrm{Int} = \int\int \mathrm{d}x\mathrm{d}y \frac{\exp(i\boldsymbol{pr})x}{(x^2+y^2)^{3/2}}, \tag{7}$$

By changing $x = |y|\sinh(t)$, we obtain

$$\begin{aligned}\mathrm{Int} &= 4i\int_0^\infty\int_0^\infty \frac{\sin(p_x y\sinh(t))\cos(p_y y)}{y}\frac{\sinh(t)}{\cosh^2(t)}\mathrm{d}y\mathrm{d}t \\ &= \frac{i2\pi p_x}{\sqrt{p_x^2+p_y^2}}.\end{aligned} \tag{8}$$

Putting all this together, we obtain the orbital part of the interaction as

$$H_{\mathrm{orb}} = \frac{J_{\mathrm{orb}}}{N} I_z \sum_{kk'\alpha\alpha' s} f(\boldsymbol{k},\boldsymbol{k}',\alpha,\alpha') c^+_{\boldsymbol{k}\alpha s} c_{\boldsymbol{k}'\alpha' s}, \tag{9}$$

where $J_{\mathrm{orb}} = \mu_0\hbar\gamma_{\mathrm{n}} e v_{\mathrm{F}}/2A_{\mathrm{c}}$, and

$$\begin{aligned}&f(k,k',\alpha,\alpha') \\ &\quad = \frac{(\alpha\alpha' - \exp[i(\varphi_k - \varphi_{k'})])(\alpha k + \alpha' k')}{2\sqrt{k^2+k'^2-2kk'\cos(\varphi_k-\varphi_{k'})}},\end{aligned} \tag{10}$$

and $c^+_{\boldsymbol{k}\alpha s}$ creates a quasiparticle with energy $E_\alpha(\boldsymbol{k})$ and real spin s. A closer examination of the kernel reveals that it depends only on the relative angle of the incoming and outgoing momenta $(\varphi_k - \varphi_{k'})$ and on the ratio of the absolute values of momenta (k/k'). At low temperatures, only electrons living close to the chemical potential matter, *i.e.*, $E_\alpha(\boldsymbol{k}) \approx E_{\alpha'}(\boldsymbol{k}')$, which leads to $k \sim k'$ and $\alpha = \alpha'$. The interaction is bounded as $|f(\boldsymbol{k},\boldsymbol{k}',\alpha,\alpha')| \leq 1$. The magnitude of the orbital term can be estimated as $J_{\mathrm{orb}} \approx 21\,\mathrm{MHz}$ using $\gamma(^{13}\mathrm{C})/2\pi = 10.7\,\mathrm{MHz/T}$.

We note, that the comparison of Eqs. (1) and (5) allows to identify formally the effective orbital Bohr magneton of massless Dirac fermions as $\mu_{\mathrm{B}}^* \sim e v_{\mathrm{F}} a$. Interestingly, it can be understood from classical considerations: a particle with charge e moving on a circular orbit with radius r and velocity v induces a magnetic moment $m = evr/2$ that is similar to the above value of μ_{B}^* after identifying $r \sim a$.

3 Nuclear spin relaxation time and Knight shift The effective interaction describing the HFI in graphene is obtained from Eq. (5) as

$$H_{\mathrm{HFI,graphene}} = \boldsymbol{S}\overline{\boldsymbol{A}}\boldsymbol{I} + H_{\mathrm{orb}}, \tag{11}$$

where $\overline{\boldsymbol{A}}$ is a 3×3 tensor with diagonal elements. Of these, the traceless elements are due to the spin dipole interaction as $A_{\mathrm{dip}}(x,y) : A_{\mathrm{dip}}(z) = -A_{\mathrm{dip}} : 2A_{\mathrm{dip}}$ and the scalar term, A_{iso}, is given by the isotropic Fermi contact interaction. First principles calculations [13] gave $A_{\mathrm{dip}} = 73\,\mathrm{MHz}$ and $A_{\mathrm{iso}} = -44\,\mathrm{MHz}$, which gives $(-117,-117,102)\,\mathrm{MHz}$ for the diagonal elements of $\overline{\boldsymbol{A}}$. We note that the first principles value of A_{dip} agrees well with the $A_{\mathrm{dip}} = 91\,\mathrm{MHz}$ is obtained for the p_z orbital of a free carbon atom [1, 14], which confirms that it is indeed the relevant orbital in graphene.

For a given direction of the magnetic field, terms of Eq. (11) perpendicular to the field contribute to relaxation and terms parallel to it contribute to the Knight shift [6, 12]. The orbital interaction involves only I_z, thus it affects T_1 when the magnetic field is applied within the graphene plane $(x-y)$, but it does not influence the Knight shift. In a magnetic field perpendicular to the graphene plane, the orbital interaction cannot flip the nuclear spin and does not cause relaxation. Also its contribution to the Knight shift vanishes.

The spin-lattice relaxation rate and the Knight shift, K, in a given direction $(i = x, y, z)$ of the magnetic field are [15]

$$\left(\frac{1}{T_1 T}\right)_i = \frac{C_i^2 \pi k_{\mathrm{B}}}{\hbar}\int_{-\infty}^{\infty} \frac{\rho(E-h_{\mathrm{Z}})\rho(E+h_{\mathrm{Z}})\mathrm{d}E}{4k_{\mathrm{B}}T\cosh^2[(E-\mu)/2k_{\mathrm{B}}T]}, \tag{12a}$$

$$K_i = \frac{A_i\gamma_{\mathrm{e}}}{2\gamma_{\mathrm{n}}}\int_{-\infty}^{\infty} \frac{[\rho(E+h_{\mathrm{Z}})+\rho(E-h_{\mathrm{Z}})]\mathrm{d}E}{8k_{\mathrm{B}}T\cosh^2[(E-\mu)/2k_{\mathrm{B}}T]}, \tag{12b}$$

with $C_i^2 = \sum_{\nu\neq i}(A_\nu^2/2 + \delta_{\nu,z}2J_{\mathrm{orb}}^2)$, $\nu = x, y, z$, γ_{e} is the gyromagnetic ratio of electrons, h_{Z} the Zeeman energy of the conduction electrons, $\rho(E)$ the quasiparticle DOS, and μ is the chemical potential. T_1 and K along an arbitrary direction is readily obtained by usual angular dependent combinations [12]. The orbital interaction contributes to Eq. (12a) by an additional term proportional to $2J_{\mathrm{orb}}^2$ for in plane field (the factor 2 comes from the spin degeneracy), on top of the spin interactions. The relaxation time for out of plane field due to spin–spin interaction (*without the orbital term*) would be 15% shorter than for in plane fields. However, the orbital interaction shortens the relaxation time for in plane field, which could result in an almost isotropic nuclear spin relaxation or a shorter in plane relaxation than for perpendicular field. More precise statements would require the first principles calculation [13] of J_{orb}. The Knight shift changes sign from in plane to out of plane fields, and drops by 15% in magnitude. We drop the i index from C_i in the following.

The magnitude of Zeeman energy is below 1 meV that is always smaller than one of $k_{\mathrm{B}}T$, μ, or Γ (the latter is due to impurities), which allows us to neglect it in the following. For ultra-clean samples at low temperature and in the vicinity of the Dirac point (DP), the Zeeman energy replaces μ.

We distinguish two scenarios for the DOS: (i) absence of Landau levels and (ii) where the presence of Landau levels is important. Scenario (i) occurs for three cases: when the magnetic field is in the plane, when the magnetic field is arbitrary but level broadening due to Γ or the temperature makes the Landau levels undistinguishable around μ [the criterion is $v_{\mathrm{F}}^2 eB\hbar/\mu \leq \max(\Gamma, k_{\mathrm{B}}T)$], or in the vicinity of

the DP point (*i.e.*, μ is small) when the lowest Landau level is significantly broadened due Γ or the temperature [the criterion is $v_F\sqrt{2eB\hbar} \leq \max(\Gamma, k_BT)$].

For scenario (i), the magnetic field-free DOS can be used to evaluate the above expressions and it reads as:

$$\rho(E) = \frac{A_c|E|}{2\pi\hbar^2 v_F^2}, \tag{13}$$

in units of states/(eV · spin · C-atom). The resulting relaxation rate using the Dirac description is

$$\left(\frac{1}{T_1T}\right) = C^2\frac{\pi k_B}{\hbar}\left[\rho^2(\mu) + \rho^2\left(\frac{\pi k_BT}{\sqrt{3}}\right)\right], \tag{14}$$

which increases as $\max(\mu^2, (\pi k_BT)^2/3)$. Away from the DP, the chemical potential dominates, and the temperature becomes important only upon approaching the DP.

Exactly at the DP, the relaxation time diverges as $T_1 \sim T^{-3}$, therefore the nuclear spins are not relaxed by conduction electrons at $T = 0$ due to the absence of charge carriers at the charge neutrality point. In the presence of impurities, the DOS reads as [16]

$$\rho_\Gamma(E) = \frac{A_c}{2\pi\hbar^2 v_F^2}\left[-\frac{\Gamma}{\pi}\ln\left(\frac{E^2+\Gamma^2}{D^2}\right) + |E|\left(1-\frac{2}{\pi}\arctan\left(\frac{\Gamma}{|E|}\right)\right)\right], \tag{15}$$

with Γ the scattering rate and D the cutoff in the continuum theory. Therefore, the aforementioned divergence of the clean system weakens to $T_1 \sim (\Gamma^2\ln^2(D/\Gamma)T)^{-1}$, reproducing the Fermi-gas behavior. Since the DOS is finite at the DP due to impurities, the Dirac nature of the quasiparticles is lost at this level.

The Knight shift is evaluated as

$$K = A\frac{\gamma_e}{2\gamma_n}\rho\left(2k_BT\ln\left[2\cosh\left(\frac{\mu}{2k_BT}\right)\right]\right). \tag{16}$$

It can be approximated by $K \sim \max(2k_BT\ln 2, |\mu|)$. Impurities provide a finite DOS even at the DP, therefore the Knight shift stays finite there as $K \sim \Gamma\ln(D/\Gamma)$.

Concluding scenario (i), we give $1/T_1T$ for two special cases: graphene biased with a gate and graphene intercalated with alkali atoms. For gate biasing, the density of charge carriers, n is controlled by the gate voltage, V_g through [17] $n = \alpha V_g$ with $\alpha = 7.2\times10^{10}\,\mathrm{cm}^{-2}/\mathrm{V}$. When $\mu \gg k_BT$ the nuclear spin relaxation rate is

$$\left(\frac{1}{T_1T}\right) = \frac{k_BC^2A_c^2}{4\hbar^3v_F^2}\alpha V_g \approx 4\times10^{-8}V_g\left[(\mathrm{VKs})^{-1}\right]. \tag{17}$$

For scenario (ii), Landau level formation is important, and the continuous spectrum is replaced by discrete Landau levels as $E_{n\alpha} = \alpha E_L\sqrt{n}$ where $\alpha = \pm$, n is non-negative integer, $E_L = v_F\sqrt{2\hbar eB_z}$ is the Landau scale, and B_z is the perpendicular component of the magnetic field. With this, the DOS reads as [16]

$$\rho(E) = \frac{A_c}{2\pi\hbar^2v_F^2}\frac{1}{2\pi}\left[\frac{\Gamma E_L^2}{E^2+\Gamma^2} - 4\Gamma\ln\left(\frac{E_L}{D}\right) - 2\mathrm{Im}\left\{(E+i\Gamma)\Psi\left(1-\frac{(E+i\Gamma)^2}{E_L^2}\right)\right\}\right], \tag{18}$$

where $\Psi(x)$ is Euler's digamma function, and reduces to Eq. (14) for clean systems with vanishing magnetic field. The nuclear spin relaxation rate and the Knight shift are plotted in Fig. 2 separately as a function of the chemical potential. These display the characteristic de Haas–van Alphen like oscillatory behavior at high magnetic field and low chemical potential and temperature, that we refer to as the extreme quantum limit (EQL).

4 Korringa relation Calculation of the relaxation rate and Knight shift allows to test the validity of the Korringa relation, *i.e.*, whether $1/T_1TK^2 = \mathrm{const}$ holds. The Korringa relation is valid for a Fermi-liquid. For non-interacting fermions, its value is given by

It is shown in Ref. [18] that neither dipolar nor orbital anisotropy affects the Korringa relation $(1/T_1TK^2)_F = 4\pi k_B(\gamma_n/\gamma_e)^2/\hbar$. For Dirac electrons and for scenario (i), in the limit of $(\mu, k_BT) \gg (\Gamma, h_Z)$, which is referred to as the scaling limit, it reads as

$$\frac{1}{T_1TK^2} = \frac{4\pi k_B}{\hbar}\left(\frac{\gamma_n}{\gamma_e}\right)^2\left(\frac{C^2}{A^2}\right)F\left(\frac{\mu}{k_BT}\right), \tag{19}$$

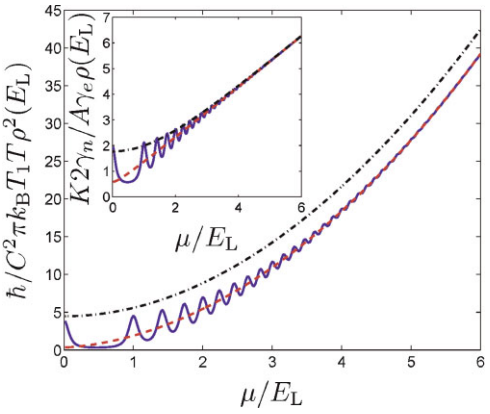

Figure 2 (online color at: www.pss-b.com) The nuclear spin relaxation rate (main figure) and the Knight shift (inset) are shown with $\Gamma = 0.1E_L$ and $D = 1000E_L$ as a function of the chemical potential. The blue solid/red dashed line refers to the presence/absence of magnetic field at $T = 0$, the black dash-dotted line corresponds to $k_BT = E_L$ in the presence of magnetic field. Increasing μ or T makes the Landau level structure disappear, and scenario (ii) is replaced by scenario (i).

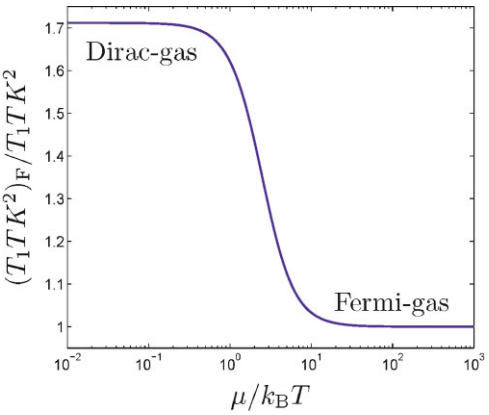

Figure 3 (online color at: www.pss-b.com) The Korringa relation, normalized to its Fermi-gas value, is shown. It satisfies to usual Korringa relation for $x \gg\gg k_BT$, and exhibits additional terms for $\mu \sim k_BT$. For large T, it enhances and saturates to a $\pi^2/3\ln^2(4)$ times bigger value.

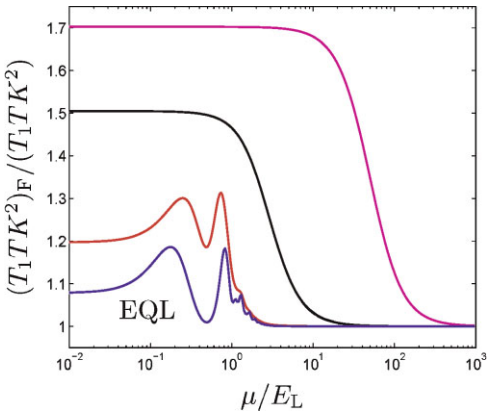

Figure 4 (online color at: www.pss-b.com) The Korringa relation, normalized to its Fermi-gas value, is shown in the presence of Landau levels for $\Gamma = 0.1E_L$, which allows for the visibility of independent Landau levels for small level index. The temperature was varied as $k_BT/E_L = 0.05$, 0.1, 1, and 20 from bottom to top. For temperatures comparable to Γ, separate peaks indicate the Landau level structure, and the curves cross over to the field-free scaling limit with increasing T.

which depends only on the ratio of μ and T, and $F(x)$ is a universal scaling function

$$F(x) = \frac{3x^2 + \pi^2}{12\ln^2[2\cosh(x/2)]}, \tag{20}$$

which is even in x and satisfies $F(0) = \pi^2/3\ln^2(4) \approx 1.71$ and $F(\infty) = 1$, and is shown in Fig. 3. For in-plane field, $C^2/A^2 < 1$, while for perpendicular field, $C^2/A^2 > 1$ due to the orbital contribution to relaxation. For $\mu \gg k_BT$, the DOS is finite, and nothing distinguishes graphene from a conventional metal because only one branch of the "V"-shaped dispersion is seen due to the smallness of T, therefore the usual Korringa relation is satisfied. On the other hand, in the opposite limit ($\mu \ll k_BT$), the Korringa relation leads to a constant, $F(0)$ times bigger than its conventional value, signaling the nature of Dirac fermions. The crossover can be explored even away from the DP by fixing the chemical potential to a finite value, and sweeping the temperature. Right at the DP, impurities spoil the crossover and re-establish the Fermi-gas relation for $(k_BT, \mu) \ll \Gamma$.

The Korringa relation is shown in Fig. 4 in a magnetic field, extrapolating between scenario (i) and (ii). For small temperatures and broadening, the discrete Landau level structure is visible in the DOS for small energies, thus oscillatory behavior characterizes the Korringa relation. When $(k_BT, \Gamma) > E_L$, the Landau levels are smeared and the presence of magnetic field does not play an important role. Fig. 5 summarizes our findings on the NMR properties. The EQL shows up only at low temperatures and small chemical potential, when the Landau level structure is visible. Larger Γ favors the Fermi gas region.

5 Realization of NMR experiments on graphene NMR is generally considered as one of the least sensitive experimental tools albeit its tremendous utility. For graphene, the expected low sensitivity stems from the low abundance (1.1%) of the NMR active ^{13}C nuclei in natural carbon and its low gyromagnetic ratio, $\gamma(^{13}\mathrm{C}) \approx \gamma(^{1}\mathrm{H})/4$. NMR spectrometer performance is characterized by the limit of detection (LOD) parameter, *i.e.*, the number of nuclei in the sample required to give a signal-to-noise ratio of three in a single acquisition. State-of-the-art spectrometers [19] have $\mathrm{LOD}_0 = 10^{12}/\sqrt{\mathrm{Hz}}$ for ^{1}H spins where the sample and detector are at room temperature in a 14 T magnetic field ($\nu(^1\mathrm{H}) = 600$ MHz). For a general case the LOD is [20]:

$$\mathrm{LOD} = \frac{\mathrm{LOD}_0}{c}\sqrt{\frac{1\ \mathrm{sec}}{T_2^*}}\left(\frac{\gamma(^1\mathrm{H})}{\gamma}\right)^3 \frac{T_s}{300\ \mathrm{K}}\mathrm{NF}_{\mathrm{rel}}. \tag{21}$$

Here c is the abundance of the given nucleus, T_2^* is the apparent decay time of the NMR signal which contains the spin–spin relaxation time, T_2, and the magnetic field inhomogeneity due to defects and the magnet. The NMR

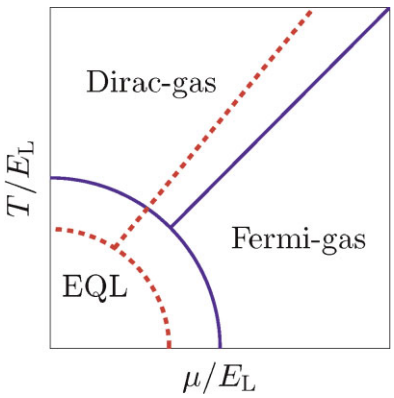

Figure 5 (online color at: www.pss-b.com) The schematic "phase diagram" of graphene according to NMR, the phases are separated by solid lines. The boundaries denote crossovers. With increasing disorder, the solid lines move to the dashed ones, and the Fermi gas region gains territory.

signal intensity follows the Curie temperature dependence of the nuclear magnetization, that is described by the sample temperature, T_s. NF_{rel} is the receiver noise factor relative to a receiver at 300 K.

Equation (21) gives that NMR would require a prohibitively large graphene sheet unless (i) a high (nearly 100%) ^{13}C isotope enrichment, (ii) low ($\sim$1 K) sample temperature and low detector noise factor are achieved. Isotope enriched carbonaceous nanostructures such as fullerenes [21] and carbon nanotubes [22] were reported and synthesis of highly ^{13}C enriched graphene sheets with a sizeable area appears feasible in particular with the vapor deposition method [23]. Low sample temperatures are customary in solid state NMR and the cryo-probe NMR [24] reported a factor 8 decrease, *i.e.*, $NF_{rel} = 1/8$ in the detector noise. We estimate that the FWHM $= 1/\pi T_2^*$ is 50 ppm at 14 T of fully ^{13}C enriched graphene giving $T_2^* = 10\,\mu s$. This is based on results of ^{13}C enriched fullerenes [25] and carbon nanotubes [22], provided either a single graphene sheet or a set of graphene layers oriented alike are present.

These factors give an LOD for ^{13}C graphene of $LOD_{graphene} = 8 \times 10^{12}$ which corresponds to a surface of 0.63 mm^2. We think that synthesis of a fully ^{13}C isotope enriched graphene with such an area (not necessarily of a single piece) is within reach. The above is a conservative estimate and we expect that a dedicated NMR microcoil setup, prepared by lithographic methods [19] would decrease the LOD value and the required graphene sheet area.

6 Conclusions In summary, we generalized the canonical theory of HFI between nucleus and conduction electrons for the case of massless Dirac fermions. The orbital part of the HFI differs from its usual form. The NMR measurables are calculated as a function of the chemical potential, temperature, and the magnetic field and we identified the fingerprints of the Dirac gas and EQL regions in the NMR parameters as opposed to the usual Fermi liquid state. We argue that NMR studies on graphene are within realistic reach.

Acknowledgements We acknowledge useful discussions with P. Thalmeier, A. Ványolos, and T. Ma. This work was supported by the Hungarian Scientific Research Fund under grant numbers OTKA K72613 and F61733. B. D. acknowledges the Bolyai program of the Hungarian Academy of Sciences for support.

References

[1] C. P. Slichter, Principles of Magnetic Resonance, 3rd ed. (Spinger-Verlag, New York, 1989).
[2] K. Wüthrich, Acta Crystallogr. D Biol. Crystallogr. **51**, 249–270 (1995).
[3] N. A. Gershenfeld and I. L. Chuang, Science **275**, 350–356 (1997).
[4] I. L. Chuang, L. M. K. Vandersypen, X. L. Zhou, D. W. Leung, and S. Lloyd, Nature **393**, 143–146 (1998).
[5] L. C. Hebel and C. P. Slichter, Phys. Rev. **113**, 1504–1519, (1959).
[6] A. Abragam, Principles of Nuclear Magnetism (Clarendon Press, Oxford, 1961).
[7] K. S. Novoselov, A. K. Geim, S. V. Morozov, D. Jiang, Y. Zhang, S. V. Dubonos, I. V. Grigorieva, and A. A. Firsov, Science **306**, 666 (2004).
[8] A. H. Castro Neto, F. Guinea, N. M. Peres, K. S. Novoselov, and A. K. Geim, Rev. Mod. Phys. **81**, 109 (2009).
[9] P. Lee and N. Nagaosa, Phys. Rev. B **43**, 1223 (1991).
[10] J. J. van der Klink and H. P. Brom, Prog. Nucl. Magn. Reson. Spectrosc. **36**, 89 (2000).
[11] J. Cserti and Gy. Dávid, Phys. Rev. B **74**, 172305 (2006).
[12] J. Winter, Magnetic Resonance in Metals (Clarendon Press, Oxford, 1971).
[13] O. V. Yazyev, Nano Lett. **8**, 1011 (2008).
[14] N. Sato, H. Tou, Y. Maniwa, K. Kikuchi, S. Suzuki, Y. Achiba, M. Kosaka, and K. Tanigaki, Phys. Rev. B **58**, 12433 (1998).
[15] T. Moriya, Prog. Theor. Phys. **28**, 371 (1962).
[16] S. G. Sharapov, V. P. Gusynin, and H. Beck, Phys. Rev. B **69**, 075104 (2004).
[17] A. K. Geim and K. S. Novoselov, Nature Mater. **6**, 183 (2007).
[18] V. P. Antropov, I. I. Mazin, O. K. Andersen, A. I. Liechtenstein, and O. Jepsen, Phys. Rev. B **47**, 12373 (1993).
[19] P. J. M. van Bentum, J. W. G. Janssen, A. P. M. Kentgens, J. Bart, and J. G. E. Gardeniers, J. Magn. Res. **189**, 104–1113 (2007).
[20] C. Massin, F. Vincent, A. Homsy, K. Ehrmann, G. Boero, P. A. Besse, A. Daridon, E. Verpoorte, N. F. de Rooij, and R. S. Popovic, J. Magn. Res. **164**, 242–255 (2003).
[21] T. W. Ebbesen, J. S. Tsai, K. Tanigaki, J. Tabuchi, Y. Shimakawa, Y. Kubo, I. Hirosawa, and J. Mizuki, Nature **355**, 620–622 (1992).
[22] F. Simon, C. Kramberger, R. Pfeiffer, H. Kuzmany, V. Zólyomi, J. Kürti, P. M. Singer, and H. Alloul, Phys. Rev. Lett. **95**, 017401–1–4 (2005).
[23] H. H. Madden and G. Hertl, Surf. Sci. **35**, 211 (1973).
[24] P. Styles, N. Soffe, C. Scott, D. Cragg, D. White, and P. White, J. Magn. Reson. **60**, 397–404 (1984).
[25] R. Tycko, G. Dabbagh, R. M. Fleming, R. C. Haddon, A. V. Makhija, and S. M. Zahurak, Phys. Rev. Lett. **67**, 1886–1889 (1991).

